

Constructing Single-atom Ni on N-doped Carbon Via Chelation-anchored Strategy for the Hydrogenolysis of Lignin

Li Tianjin¹, Chen Bo¹, Cao Meifang¹, Ouyang Xinping¹, Xueqing Qiu², and Li Changzhi¹

¹Affiliation not available

²South China University of Technology

April 13, 2022

Abstract

The utilization of lignin remains a great challenge due to its complex non-repetitive structure and the lack of efficient catalyst. Herein, a single-atom catalyst Ni@N-C was designed via a facile chelation-anchored strategy. Ni atoms were immobilized on the N-doped carbon carrier by a two-stage pyrolysis of a mixture of D-glucosamine hydrochloride, nickel acetate and melamine. D-glucosamine hydrochloride as a chelating agent prevented the aggregation of Ni²⁺, and melamine provided enough N to anchor Ni by forming Ni-N₄ structure. Ni@N-C gave a 31.2% yield of aromatic compounds from lignin hydrogenolysis, which was twice higher than that achieved by Ni cluster catalyst. Based on the experimental and DFT calculation results, the higher activity of Ni@N-C was attributed to its lower H₂ dissociation energy and the reduced energy barriers of the transition states. The strategy described opens an efficient green avenue for preparing single-atom catalyst that possesses outstanding activity in lignin depolymerization.

Constructing Single-atom Ni on N-doped Carbon Via Chelation-anchored Strategy for the Hydrogenolysis of Lignin

Tianjin Li^{1,4}, Bo Chen¹, Meifang Cao¹, Xinping Ouyang^{1*}, Xueqing Qiu², Changzhi Li^{3*}

1. School of Chemistry and Chemical Engineering, Guangdong Provincial Key Lab of Green Chemical Product Technology, South China University of Technology, Guangzhou 510640, P. R. China.

² School of Chemical Engineering and Light Industry, Guangdong University of Technology, Guangzhou 510006, P. R. China.

³CAS Key Laboratory of Science and Technology on Applied Catalysis, Dalian Institute of Chemical Physics, Dalian 116023, P.R. China.

⁴Shandong Provincial Key Laboratory of Biomass Gasification Technology, Energy Research Institute, Qilu University of Technology (Shandong Academy of Sciences), Jinan 250014, P.R. China.

*Authors to whom any correspondence should be addressed.

E-mail: ceouyang@scut.edu.cn (Xinping Ouyang); licz@dicp.ac.cn (Changzhi Li).

ABSTRACT

The efficient utilization of lignin remains a great challenge due to its complex non-repetitive structure and the lack of efficient catalyst. Herein, a single-atom catalyst Ni@N-C was designed via a facile chelation-anchored strategy. Ni atoms were immobilized on the N-doped carbon carrier by a two-stage pyrolysis of a mixture of D-glucosamine hydrochloride, nickel acetate and melamine. D-glucosamine hydrochloride as a chelating agent prevented the aggregation of Ni²⁺, and melamine provided enough N to anchor Ni by forming

Ni-N₄structure. Ni@N-C gave a 31.2% yield of aromatic compounds from lignin hydrogenolysis, which was twice higher than that achieved by Ni cluster catalyst. Based on the experimental and DFT calculation results, the higher activity of Ni@N-C was attributed to its lower H₂ dissociation energy and the reduced energy barriers of the transition states. The strategy described opens an efficient green avenue for preparing single-atom catalyst that possesses outstanding activity in lignin depolymerization.

KEYWORDS

single atom catalyst, lignin, hydrogenolysis, Ni-N₄structure, aromatic compound

1 INTRODUCTION

With the increasing demand for energy and the depletion of fossil fuels, the utilization of biomass as a renewable source for energy has drawn worldwide attention. Lignin is the most abundant renewable aromatic biopolymer on earth and has the potential to serve as a feedstock in the production of fuels and aromatic compounds^{1, 2}. However, the highly functionalized structure and robust chemical bonds of lignin greatly hamper its depolymerization for downstream utilization. It is known that lignin is composed of phenylpropane units linked by C-O and C-C bonds. The C-O bonds account for two-thirds of the total linkages between the repeating units, and have lower dissociation energy than that of the C-C bonds. Thus, a catalyst with high activity for C-O bond cleavage is the key to the successful conversion of lignin into value-added products³⁻⁶.

Many feasible methods, including hydrogenolysis, oxidation, pyrolysis, two-step strategy and photocatalysis have been proposed for lignin depolymerization⁷. From the perspective of selectivity and green chemistry, hydrogenolysis is one of the most efficient approaches⁸. Various metal catalysts based on Pd⁹⁻¹¹, Ru^{4,12,13}, Pt¹⁴⁻¹⁶, Ni^{17,18} and Re¹⁹⁻²¹, etc., have been reported for the hydrogenolysis of lignin, among which noble metal catalysts have shown good hydrogenation performance. However, undesirable over-hydrogenation is hard to avoid in noble metal-catalyzed transformation. Moreover, the high costs of the noble metals restrict their large-scale application. In light of the much lower cost and considerable catalytic activity for H₂ dissociation, Ni has been used in the hydrogenolysis of lignin. As an elegant example, Sergeev *et al*²² reported the hydrogenolysis of lignin model compound using a soluble nickel carbene complex under a mild condition (80-120 °C and 1 bar H₂) by virtue of the advantages of homogenous catalysis. To address the issues of catalyst separation and recycling, heterogeneous Ni-based catalysts such as monometallic Ni/C²³, bimetallic NiM (M=Ru, Rh, and Pd)²⁴, and Ni-Fe alloy²⁵ have also been employed in the conversion of lignin by modulation the electronic structure of Ni atoms and improving synergistic effect between Ni and the second metal species, or Ni and the support to increase catalytic efficiency. Notwithstanding, due to the inherent lower catalytic activity of Ni than that of noble metal catalysts, the hydrogenolysis of lignin over heterogenous Ni-based catalyst is usually carried out at usually high reaction temperature and high pressure, leading to side reactions such as over-hydrogenation, or fast deactivation due to the aggregation or leaching of active species.

Single-atom catalysts (SACs), with atomically dispersed metals onto the support surface, have the advantages of both “isolated sites” of homogeneous catalysts and the stability and reusability of heterogeneous catalysts, and thus are emerged as a promising frontier to bridge hetero- and homogeneous catalysis²⁶⁻²⁹. The utilization of SACs would be potentially superior alternative to the traditional hetero- and homogeneous catalysts in biomass conversion³⁰⁻³⁴. In another scenery, recent developments in metal-coordinated N-doped carbon catalysts have shown promise in selective hydrogenation³⁵. The strong electronic interaction between metal atoms and N atoms accelerates the electron transfer in the catalytic system, resulting in improved activity and stability of the catalyst³⁶. In view of the advantages of SACs, and the fact that the electronic structure of active sites is the key factor for affecting the hydrogenolysis activity of a catalyst in lignin depolymerization²³, it is assumed that design of atomically dispersed Ni on N-doped carbon material with electronic interaction between Ni and N atoms might be promising catalysts for lignin decomposition.

Herein, a facile chelation-anchored strategy is developed for the construction of a single-atom Ni@N-C catalyst with a high-Ni loading via a two-stage pyrolysis of a mixture of D-glucosamine hydrochloride, nickel

acetate and melamine, which are individually served as chelating agent, metal precursor and soft-template, respectively. This catalyst exhibits much higher catalytic activity and durability than the commercial Pd/C catalyst and N-doped carbon supported Ni nanoparticles (Ni@NC) in the hydrogenolysis of lignin into aromatic compounds, demonstrating the application potential of SACs in the conversion of complex biopolymers.

2 MATERIALS AND METHODS

2.1 Materials

All chemicals used were analytical grade without further purification. Glucosamine hydrochloride, melamine, Ni(OAc)₂*4H₂O, active carbon (AC), Raney nickel and Ru/C were purchased from Aladdin Chemistry Co. Ltd (China). 2-phenoxy-1-phenethanol, phenethoxybenzene, phenol, ethylbenzene, phenylethyl alcohol were purchased from Alfa Aesar Co. Inc. (China). Birch wood was purchased from Shandong wood Co. Ltd. (China).

2.2 Synthesis of Ni@N-C SAC

A total of 1 g Ni(OAc)₂*4H₂O was combined with 20 g melamine and D-glucosamine hydrochloride followed with thorough mixing. The mixture was then placed in a ceramic boat and calcined with a two-stage pyrolysis procedure: The temperature was raised to 600 degC with a heating rate of 2.0 degC/min and hold for 1 h; After that, the temperature was further raised to 800 degC with the same heating rate; Finally, the sample was cooled down to room temperature. For comparison, Ni@NC was synthesized by the above method without the addition of melamine. Similarly, 1 g D-glucosamine hydrochloride was directly calcined at 800 degC for 1h, the obtained sample was co-pyrolyzed with Ni(OAc)₂*4H₂O and melamine using the same process as the Ni@N-C SAC and the resultant sample was named as Ni@C. The contrastive samples were synthesized in parallel by the same method as that for Ni@N-C SAC except for the chitosan/lignin instead of D-glucosamine hydrochloride.

2.3 Synthesis of Ni NPs deposited on AC

The catalyst of Ni@AC was prepared by the wetness impregnation method. Ni(OAc)₂*4H₂O (0.1106 g) was first dissolved in 20 mL deionized water, and then 0.3 g of AC was added to the Ni solution. The resulting slurry was stirred for 24 h and then dried in oil bath at 80 degC. The dried slurry was subjected to a heating process in a tube furnace with an H₂/N₂(1:9) gas flow at a flow rate of 100 mL/min. The tube furnace was programmed as follows: raise to 120 degC at 2 degC/min and hold for 20 min; then further raise to 400 degC at 1 degC/min, cool down to room temperature.

2.4 Characterization of Catalysts

X-ray diffraction (XRD) was collected on a Rigaku diffractometer (D/MAX, 3 kW) equipped with Cu K α radiation (40 kV, 30 mA, λ =0.1543 nm) (Bruker, Germany) and the patterns were recorded in the 10-90 $^{\circ}$. X-ray photoelectron spectroscopy (XPS) was carried out on a Kratos Axis Ultra DLD system. Transmission electron microscopy (TEM) was performed using a JEOL Model 2100F electron microscopy at 200 kV. Aberration-corrected scanning STEM images were taken using a Cs-corrected FEI Titan G2 60-300 Microscope operated at 300 KV using an HAADF detector. Field emission scanning electron microscopy (FFSEM, Merlin, Germany) was performed to measure the morphology of the samples. The X-ray absorption spectra were collected on the beamline BL01C1 in NSRRC. The radiation was monochromatized by a Si (111) double-crystal monochromator. X-ray absorption near-edge structure (XANES) and extended X-ray absorption fine structure (EXAFS) data reduction and analysis were processed by Athena software. N₂ adsorption isotherms of catalysts at 77K were measured on a Tristar II 3020, USA. The samples were pretreated at 200 $^{\circ}$ C for 12 h under vacuum. The metal content of the catalysts was confirmed by Perkin-Elmer TJA RADIAL IRIS 1000.

2.5 Decomposition of Lignin Model Compounds

0.1 g (0.467 mmol) lignin model compound, 0.02 g catalyst and 20 mL water/ethanol (1:1) were added into the 100 mL stainless steel autoclave (Beijing Shijisenlang Chemical Machinery Co., Ltd., China). The

autoclave was purged with N₂ for three times and the pressure was increased to 1MPa hydrogen. And the catalytic reaction was carried out at 200 °C for 5 h. After reaction, the mixture was filtered to remove catalyst. The organic products were extracted with ethyl acetate and analyzed by gas chromatography-mass spectrometry (GC-MS). The conversion of model compounds and the yield of products were calculated using the following Eq. (1) and Eq. (2):

$$\text{Conversion (\%)} = W_R/W_S \times 100\% \quad (1)$$

$$\text{Yield of product } i \text{ (\%)} = n_i / n_m \times 100\% \quad (2)$$

Where W_R is the weight of reacted after the hydrogenolysis of lignin model compound; W_S is the weight of substrate (0.1 g); where n_i and n_m are the moles of product i and initially added compound (0.467 mmol), respectively.

2.6 Lignin Hydrogenolysis

The hydrogenolysis of birch organosolv lignin was carried out in 100 mL stainless steel autoclave (Beijing Shijisenlang Chemical Machinery Co., Ltd., China). Typically, 0.3 g birch organosolv lignin 0.06 g catalyst and 20 mL water/ethanol (1:1) were added into the autoclave vessel. The vessel was purged three times with nitrogen before sealed and pressured to 1 MPa with hydrogen. The reaction was carried out at 280 °C for 2 h. After reaction, the reaction vessel was cooled to room temperature. The reaction mixture was filtered to remove catalyst and the filtrate was extracted with ethyl acetate to obtain lignin oil. And then, the lignin oil was analyzed by GC-MS, gel permeation chromatography (GPC) and two-dimensional heteronuclear single quantum correlation (2D HSQC). The yield of the aromatic monomers was calculated using the following Eq. (3):

$$\text{Yield of the aromatic monomers (\%)} = W_A/W_F \times 100\% \quad (3)$$

Where W_A is the weight of aromatic monomers after the hydrogenolysis of lignin; W_F is the weight of feed lignin.

2.7 Analysis of Products

GC-MS was performed with an Agilent 5975C-7890A equipped with a capillary column (HP-5MS 30 m×mm×0.25 μm) and EI ion source (70 eV). The following operating condition was used: a column temperature program of 50 °C (3 min), 7 °C/min to 150 °C, 150 °C for 10 min, 20 °C /min to 300 °C, 300 °C for 20 min. GPC analysis was performed with a Waters 1515/2414 liquid chromatography system (Waters 1515/2414, Waters Co., USA). The tetrahydrofuran (THF) was used as the eluent. The lignin and depolymerized products were dissolved in THF at a concentration of 5 mg mL⁻¹. The 2D HSQC was performed on a Bruker AV 600 MHz spectrometer. And 100 mg of lignin and lignin oil were dissolved in 0.5 mL DMSO-d₆.

2.8 DFT Calculations

The present first principle DFT calculations are performed with the projector augmented wave (PAW) method^{37,38} in Vienna ab initio simulation package (VASP). The exchange-functional is treated using the generalized gradient approximation (GGA) of Perdew-Burke-Ernzerhof (PBE)³⁷ functional. The cut-off energy of the plane-wave basis is set at 450 eV for optimize calculations of atoms and cell optimization. The vacuum spacing in a direction perpendicular to the plane of the catalyst is at least 12 Å. The Brillouin zone integration is performed using 4×4×1 Monkhorst-Pack k-point sampling for a primitive cell³⁹. The self-consistent calculations apply a convergence energy threshold of 10⁻⁵ eV. The equilibrium lattice constants are optimized with maximum stress on each atom within 0.03 eV/Å. The Hubbard U (DFT+U) corrections for 3d transition metal by setting according to the literature⁴⁰. The binding energy is calculated using the following Eq (4):

$$E_{\text{ads}} = E_{\text{total}} - (E_m + E_1) \quad (4)$$

where the E_{total} is the energy of structure with adsorbed structure, E_m is the energy of N-doped carbon structure, E_1 is the energy of the single atom or clusters.

The free energy was calculated using the following Eq (5):

$$G=E+ZPE-TS \quad (5)$$

where G, E, ZPE and TS are the free energy, total energy from DFT calculations, zero point energy and entropic contributions (T was set to be 298K), respectively.

3 RESULTS

3.1 Chelation-anchored strategy for constructing Ni@N-C SAC

The Ni@N-C SAC was prepared by the mean of a two-stage pyrolysis of a mixture of D-glucosamine hydrochloride, nickel acetate and melamine, which were individually served as chelating agent, metal precursor and soft-template, respectively (Figure 1a). In the first stage (<600 °C), the thermal condensation of melamine produced graphite carbon nitride (g-C₃N₄), and thermal degradation of D-glucosamine hydrochloride formed a carbon skeleton between g-C₃N₄ layers⁴¹. In the second stage, g-C₃N₄ began thermolysis at a temperature above 700 °C and finally formed N-doped graphene-like nanosheets, providing a nitrogen source for the formation of Ni-N_x structure when the temperature reached 800 °C. The morphology of Ni@N-C SAC was characterized by SEM and TEM.

As shown in Figure 1b and 1c, Ni@N-C SAC is composed of wrinkled graphene-like nanosheets. The TEM image of Ni@N-C SAC only shows one atom lattice structure (d=3.52 Å), which is attributed to graphite carbon (Figure 1d). The XRD spectrum of the Ni@N-C SAC has two broad peaks at 26.3° and 41.2°, which are corresponding to 002 peak and 100 peak of graphitic carbon⁴², while diffraction peaks of Ni are not detected (Figure S1). However, aberration-corrected high-angle annular dark field scanning transmission electron microscopy (HAADF-STEM) shows that Ni single atoms are homogeneously distributed across the wrinkled graphene-like nanosheets (Figure 1e-f). And the average diameter of the spots is 1.67 ± 0.29 Å based on the statistical analysis of over 100 bright spots (the top right corner of Figure 1f). In addition, the EDS-mapping analysis reveals the homogeneous distribution of Ni, N and C atoms across the whole graphene-like nanosheets (Figure 1g). These above results indicate that Ni is atomically distributed on the carrier.

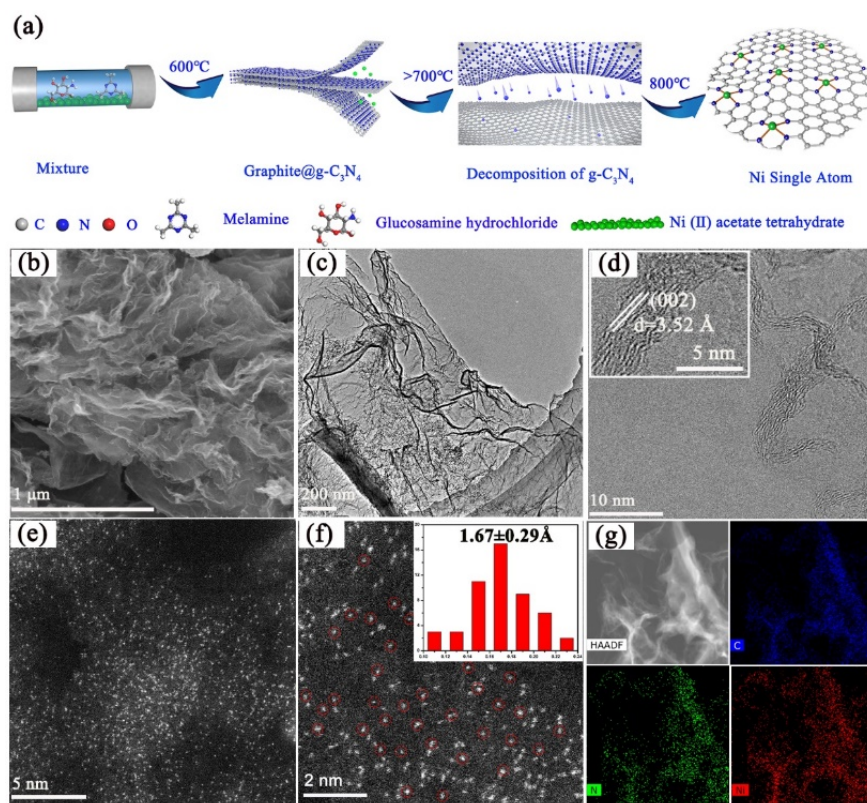


FIGURE 1 Synthesis and characterizations of Ni@N-C SAC: (a) Schematic illustration of the synthesis process of Ni@N-C SAC. (b) SEM image. (c) TEM image. (d) HRTEM image. (e, f) Aberration corrected HAADF-STEM image. (g) EDX elemental mapping.

3.2 Electronic structure of Ni atoms in Ni@N-C SAC

The XPS was used to characterize the chemical composition and valence state of Ni@N-C SAC (Figure S2). The binding energy of the Ni 2p_{3/2} peak is 855.1 eV, which is higher than that reported for Ni⁰ (853.4 eV) and lower than that for Ni²⁺ (855.7 eV)^{43, 44}. The high-resolution XPS N 1s spectrum can be deconvoluted into pyridinic N (398.1 eV), Ni-N (399.2 eV), pyrrolic N (400.4 eV), graphite N (401.3 eV) and N-oxidized (403.0 eV)⁴⁵. Based on the XPS data (Table S1), the atomic concentration of Ni in Ni@N-C SAC is 8.01 wt%.

To further study the electronic structures of Ni species in Ni@N-C SAC, the analysis of XANES and EXAFS was conducted. Figure 2a shows the Ni K-edge XANES spectra of Ni@N-C SAC and two references: Ni foil and NiO. In the first derivative XANES spectra, the intensity lines (absorption edges) of Ni@N-C SAC lie between those of Ni foil and NiO, demonstrating the unique electronic structure of Ni^{δ+} (0 < δ < 2) in Ni@N-C SAC, where the valence of the Ni species is between Ni⁰ and Ni²⁺. This observation is consistent with the aforementioned XPS results. The Fourier transform of the k³-weighted Ni K-edge EXAFS spectrum of Ni@N-C SAC exhibits a dominant peak at 1.41 Å, corresponding to the Ni-N coordination, which is shorter than both the Ni-O peak in the NiO spectrum and the Ni-Ni peak in the Ni foil spectrum (Figure 2b). The wavelet transform was also employed to assess the Ni K-edge EXAFS oscillations of Ni@N-C SAC. As shown in Figure 2c, the wavelet transform analysis of Ni@N-C SAC displays only one intensity maximum at 5.0 Å⁻¹, which is ascribed to the Ni-N coordination. The above results further prove the presence of atomically dispersed Ni in Ni@N-C SAC. The EXAFS fitting analysis was applied to investigate the configuration of Ni atoms in Ni@N-C SAC. The calculated coordination number of Ni is *ca* 4 and the mean bond length

of Ni@N-C SAC is 1.88 Å (Table S2). Hence, each Ni atom is confined in the N-doped carbon matrix by coordinating with four N (Ni-N₄ structure, Figure S3).

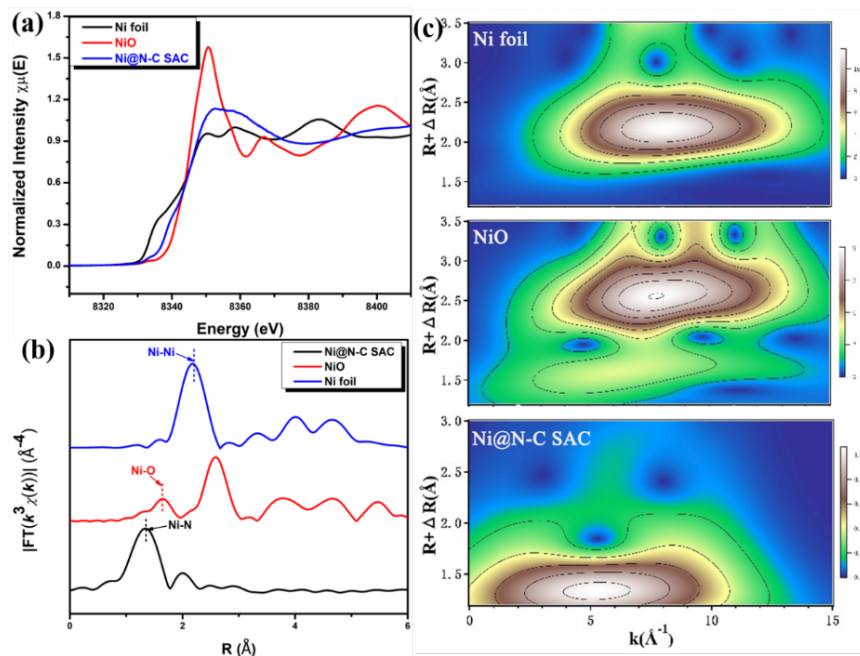


FIGURE 2 Atomic structure analysis of Ni@N-C SAC by XAFS: (a) Ni K-edge XANES spectra. (b) Fourier transform of Ni k-edge EXAFS spectra. (c) wavelet transform of k^3 -weighted EXAFS data of Ni@N-C SAC and reference samples (NiO and Ni foil).

3.3 Mechanism and universality of chelation-anchored strategy for preparing Ni@N-C SAC

The above-described morphology and electronic structure studies demonstrate the successful synthesis of Ni@N-C SAC. To investigate the role of chelating agent in synthesizing Ni@N-C SAC, D-glucosamine hydrochloride was first treated at 800 °C to remove its amino/hydroxyl groups, then the generated sample was co-pyrolyzed with nickel acetate and melamine by a standard process used in the synthesis of Ni@N-C SAC (Figure 3a), obtaining a catalyst denoted as Ni@C. SEM image of Ni@C suggests that carbon nanotubes are obtained probably via a Ni-catalyzed growth during the decomposition of melamine^{46,47} (Figure 3b). Moreover, TEM images show that a large proportion of Ni atoms aggregate to clusters rather than atomically dispersed Ni (Figure 3 c, d). The diffraction peaks of Ni@C in XRD profile at 2θ of 43.2°, 44.5°, 49.6°, 51.8° and 76.4° are attributed to NiO (012), Ni (111), Ni₂O₃ (112), Ni (200), Ni (220), respectively (Figure S4). The above results indicate that the abundant amino/hydroxyl groups of D-glucosamine hydrochloride play crucial roles to coordinate with Ni ions, which prevent the aggregation of Ni for obtaining single atom Ni.

Meanwhile, a comparison catalyst denoted as Ni@NC was prepared without the addition of melamine (Figure 3e). The SEM characterization showed that the morphology of Ni@NC (Figure 3f) was non-porous. Contrarily, Ni@N-C SAC (Figure 1b) and Ni@C (Figure 3b) display the wrinkled and porous morphology. The XRD spectrum of Ni@NC (Figure S4) shows Ni peaks obviously, and its TEM images (Figure 3 g, h) reveal that Ni clusters are formed on the carbon support.

Relying on the above studies relating the roles of chelating agent and soft-template, it could be deduced that the pyrolysis of D-glucosamine hydrochloride formed a carbon skeleton in the interlayer of the g-C₃N₄ at the lower temperature stage of pyrolysis (600 °C). The layer-by-layer stacking structure similar to sandwiches may inhibit the growth of Ni particles NPs. The further pyrolysis at a higher temperature (800 °C) produced

volatile gases from the decomposition of the $g\text{-C}_3\text{N}_4$ to form wrinkled and porous morphology. Meanwhile, decomposition of $g\text{-C}_3\text{N}_4$ resulted in the formation of active N radicals, doping into carbon skeleton and inducing the coordination of Ni with N to form Ni-N₄ structure. It should be noted that although every molecule of D-glucosamine hydrochloride contains one amino group, it cannot provide enough N to chelate Ni for hindering the aggregation of Ni in the absence of melamine. For this reason, the addition of melamine is also essential for preparing the atomically dispersed Ni species. Therefore, during the process of forming Ni SAC, the chelating agent prevents the aggregation of Ni²⁺, and the soft template provides enough N to coordinate and anchor Ni by forming Ni-N₄ structure.

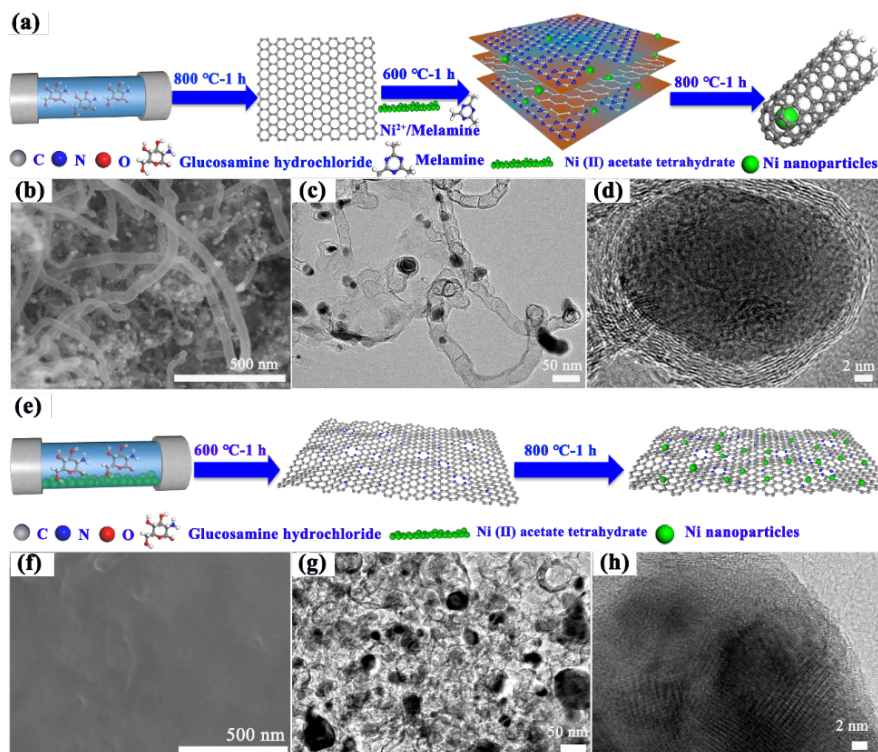


FIGURE 3 Synthesis and characterizations of control samples: (a) Scheme of the formation of Ni@C. (b) SEM images. (c, d) TEM images of Ni@C. (e) Scheme of the formation of Ni@NC. (f) SEM images. (g, h) TEM images of Ni@NC.

It is well known that lignin and chitosan are two of the most abundant biomass resources, which have rich hydroxyl groups or/and amine groups in their structures (Figure S5), suggesting the possibility that they can be used as chelating agents instead of D-glucosamine hydrochloride to synthesize Ni@N-C SAC. The aberration-corrected HAADF-STEM images of the two prepared catalysts using lignin and chitosan as chelating agents shown in Figure 4 reveal the atomically dispersed Ni sites supported on both carriers. Other characterizations of the catalysts, including SEM images (Figure S6), EDS analysis (Figure S7), together with XRD and XPS analysis (Figure S8) further reveal that Ni is atomically dispersed on the carrier of catalysts, regardless of the chelating agent is lignin or chitosan. ICP analysis indicates that Ni loading of the catalysts obtained from lignin and chitosan are 8.1 wt% and 7.5 wt%, respectively. The above results indicate that two readily available waste biomass resources are successfully used as chelating agents to synthesize Ni@N-C SAC, demonstrating that the chelation-anchored strategy is a universal method.

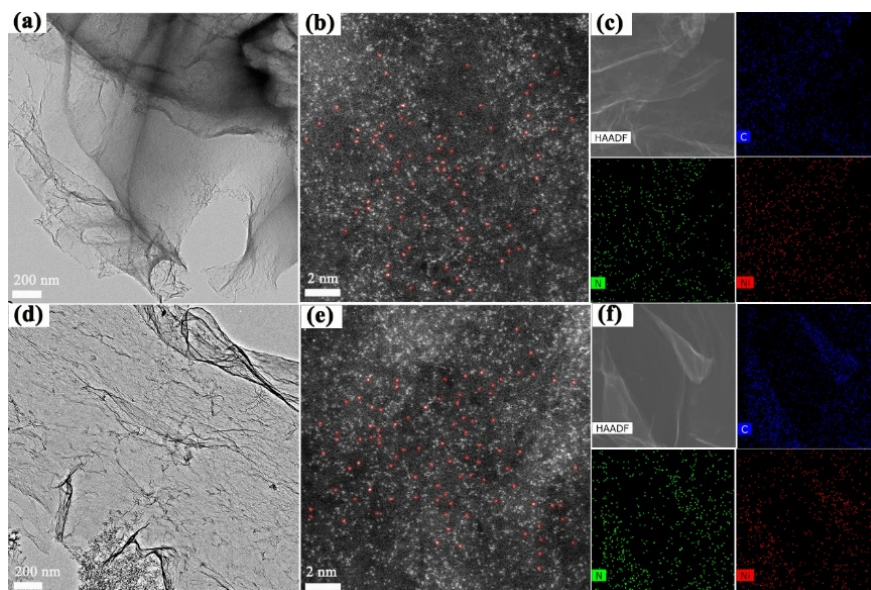


FIGURE 4 Microstructure and morphology characterizations of Ni@N-C SACs prepared by using lignin and chitosan as chelating agents: (a) TEM images. (b) Corresponding EDX elemental mapping. and (c) Aberration-corrected HAADF-STEM images of Ni@N-C SAC prepared with lignin. (d) TEM images. (e) Corresponding EDX elemental mapping and (f) Aberration-corrected HAADF-STEM images of Ni@N-C SAC prepared with chitosan.

3.4 Catalytic Performance on C-O Bond Cleavage

The catalytic performances of the synthesized catalysts were evaluated by using a typical lignin β -O-4 model compound, 2-phenoxy-1-phenethanol (PPE). Table 1 summarizes the PPE hydrogenolysis results over different catalysts. The reaction does not occur in the absence of catalyst (entry 1) and the NC support also has no catalytic activity in the reaction (entry 2). Ni@NC shows a 31% PPE conversion and a 16% phenol yield (entry 6). In sharp comparison, Ni@N-C SAC gives a much higher PPE conversion (99%) with excellent phenol yield of 92% and ethylbenzene yield of 78%. As a comparison, the commercial Raney nickel exhibits a PPE conversion of 39%, accompanying with phenol and ethylbenzene yields of 24% and 18%, respectively. The above results demonstrate clearly that Ni@N-C SAC possesses high activity in catalyzing PPE hydrogenolysis, during which the C-O bond is cleaved in the presence of H_2 . Table 1 also shows that the yield of byproduct cyclohexanol (37%) in the reaction over Pd/C catalyst is much higher than that over Ni@N-C SAC (only 1%), indicating that Ni@N-C SAC possesses high selectivity in cleaving C-O bonds without over hydrogenation of aromatic rings.

TABLE 1 Catalytic performance of various catalyst for PPE depolymerization^a.

| Entry | Catalyst | Conversion (%) | Yield (mol%) | | | | |
|-------|---------------------------|----------------|--------------|----|----|----|----|
| | | | B | C | D | E | F |
| 1 | Blank | 0 | ND | ND | ND | ND | ND |
| 2 | NC | 0 | ND | ND | ND | ND | ND |
| 3 | Raney Nickel ^b | 39 | 24 | 18 | 3 | 2 | 8 |
| 4 | Ni@N-C SAC | 99 | 92 | 78 | 8 | 1 | ND |
| 5 | Ni@C ^c | 30 | 22 | 10 | 2 | 2 | 5 |
| 6 | Ni@NC ^d | 31 | 16 | 5 | 3 | 2 | 8 |
| 7 | Ni@AC ^e | 28 | 14 | 10 | 2 | 1 | 10 |

a: Reaction conditions: PPE (100 mg), 200 °C, 5 h, catalyst (20 mg), isopropanol (20 ml), stirring at 400 rpm. b: Raney nickel was commercial purchased. c: Ni@C was prepared by pyrolyzing the D-glucosamine hydrochloride at 800 °C, the generated sample was co-pyrolyzed with nickel acetate and melamine. d: Ni@NC was prepared by the same method as the Ni@N-C SAC except that melamine was absent. e: Ni@AC was prepared by immobilizing Ni species on the commercial purchased AC via a wet impregnation method. f: Pd/C was commercial purchased and the Pd loading was 5 wt%. ND: No detected.

The DFT and molecular dynamic stimulation were employed to investigate the reason why Ni@N-C SAC is superior to Ni@NC in cleavage of the C-O bond. Based on the XANES and EXAFS results, the optimized models of Ni@N-C SAC and Ni@NC were established using VASP software (Figure 5).

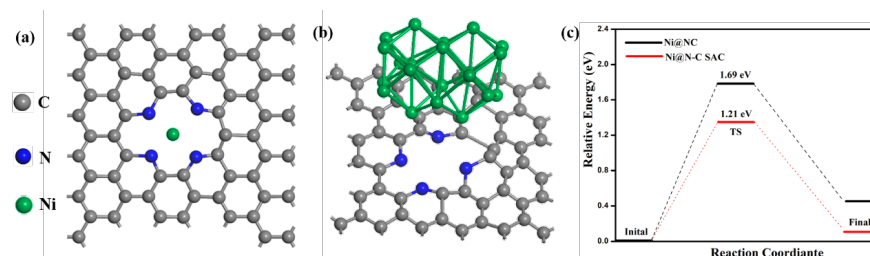


FIGURE 5 Optimized configurations of different catalysts: (a) Ni@N-C SAC. (b) Ni@NC. (c) the H₂ dissociation of energy of Ni@N-C SAC and Ni@NC.

The selective hydrogenolysis begins with the adsorption and activation of H₂⁴⁸, and then the activated hydrogen species react with PPE molecules resulting in the cleavage of the C-O bond. The calculated Ni adsorption energies were -3.17 eV for Ni@N-C SAC and -1.21 eV for Ni@NC, respectively (Figure 5a and 5b). The lower adsorption energies of Ni in the Ni@N-C SAC model suggests that Ni atoms prefer to chelate with the N atoms of the N-doped carbon support to form single-atom sites (Ni@N-C SAC) rather than aggregate with each other to form Ni clusters (Ni@NC). Moreover, the dissociation energy of molecular hydrogen on the surface of Ni@N-C SAC and Ni@NC are 1.21 eV and 1.69 eV, respectively (Figure 5c), indicating that Ni@N-C SAC contributes to more active hydrogen species, and hence exhibits higher catalytic activity.

The time course of the product distribution of PPE hydrogenolysis was monitored (Figure S9). Results shows that PPE is almost quantitatively converted to phenol, ethylbenzene and phenethoxybenzene within 150 min. Phenethoxybenzene increases initially but decreases with the prolonging of time. Therefore, phenethoxybenzene should be an intermediate for the transformation, which might be produced from the dehydration of PPE on the OH group of C_α, and it can be further hydrogenated to produce phenol and ethylbenzene by the cleavage of the aliphatic C-O bond (Figure 6a, route A). Despite there is another possible dehydration path between C_α-OH and C_β-H, the vinyl ether intermediate was not detected yet even at low temperature, we thus exclude this dehydration pathway. Phenylethyl alcohol was a minor product of the PPE hydrogenolysis, which was probably produced through the cleavage of the aliphatic C-O bond (Figure 6a, route B). The yield of phenol and ethylbenzene increases with the prolonging of the reaction time, which indicates that route A is the main reaction path of PPE hydrogenolysis.

According to the hydrogenolysis reaction pathway A, the DFT calculation of the mechanism with free energy profile was also shown in Figure 6. The reaction energy barrier diagram indicates that the two dissociated hydrogen atoms combine with the oxygen atom on C_α-OH (energy barrier: 0.979 eV) and the C_α (energy barrier: 0.354 eV), respectively, to produce phenethoxybenzene, which is further cleaved to generate phenol and ethylbenzene by overcoming the energy barriers of 0.493 eV and 0.264 eV. For Ni@NC, it was found that the energy barriers of the four transition states (TS1, TS2, TS3, and TS4) are lower than those in the

Ni@N-C SAC-catalyzed PPE hydrolysis. Therefore, Ni@N-C SAC exhibits higher catalytic activity than Ni@NC in the cleavage of C-O bonds.

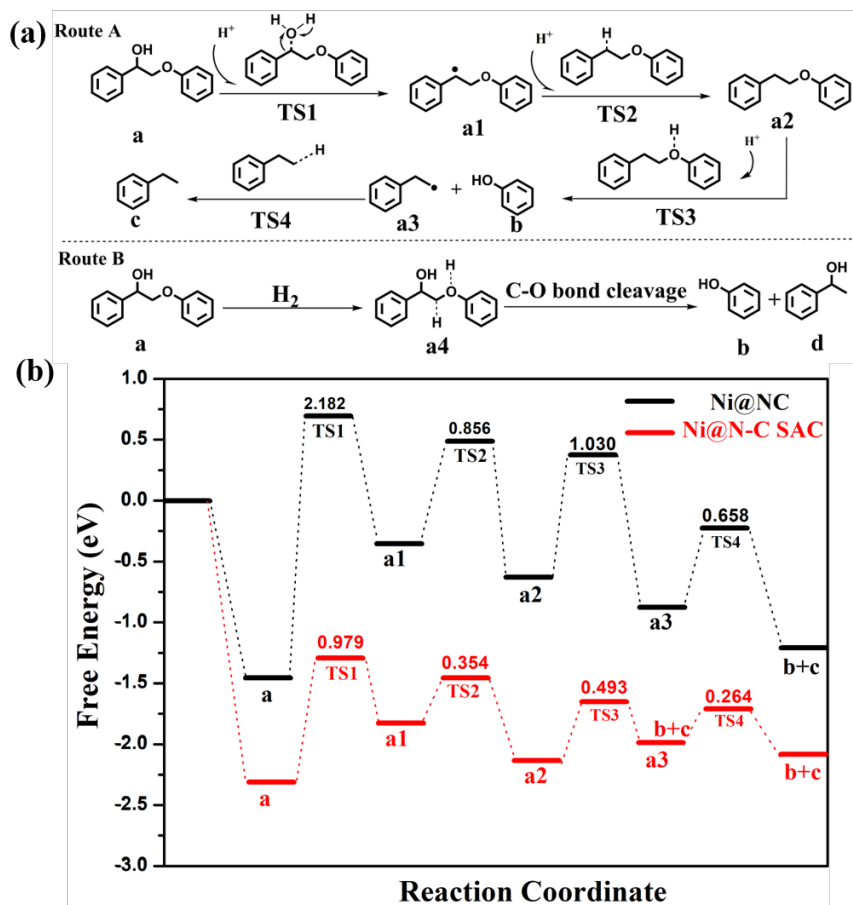


FIGURE 6 Proposed reaction path and the reaction energy barrier diagrams: (a) Proposed reaction path of PPE hydrogenolysis. (b) Reaction energy barrier of PPE hydrogenolysis by Ni@N-C SAC and Ni@NC.

To explore the range of the Ni@N-C SAC catalyst, two more β -O-4 model compounds and one α -O-4 model compound were evaluated as the substrates. It is found that benzyl phenyl ether (α -O-4) and 2-phenylethyl phenyl ether (β -O-4) over the Ni@N-C SAC are nearly completely converted, providing the corresponding phenols and arenes in high yields ([?] 80%, Table S3, entries 1-2). It is known that β -O-4 dimeric model compound with C γ -OH is structurally closer to the true lignin. Gratefully, such a model compound was also completely converted (Table S3, entry 3), affording guaiacol and 4-propylguaiacol in yields of 80% and 53%, respectively. These data demonstrated the versatility of Ni@N-C SAC in selective cleavage of the C-O bond in different lignin model compounds.

The recyclability of the Ni@N-C SAC was explored by carrying out the hydrogenolysis of PPE as listed in Figure 7a. After each run, the used catalyst was washed with ethanol following by vacuum drying. It was found that the conversion of PPE in Ni@N-C SAC-catalyzed hydrogenolysis remains unchanged after three runs. Characterizations of the used catalyst were conducted by XRD, XPS, HRTEM and aberration-corrected HAADF-STEM. There is no Ni metal diffraction peak in XRD pattern (Figure 7b). The binding energy of Ni 2p $_{3/2}$ peak (855.13 eV) of used catalyst is almost the same as that of original Ni@N-C SAC (Figure 7c). No Ni clusters or particles are observed on the surface of the used catalysts (Figure 7d, e).

Aberration-corrected HAADF-STEM characterizations show that Ni atoms were still atomically dispersed with no aggregation observed (Figure 7 f). These results demonstrate the excellent stability of Ni@N-C SAC in the hydrogenolysis systems.

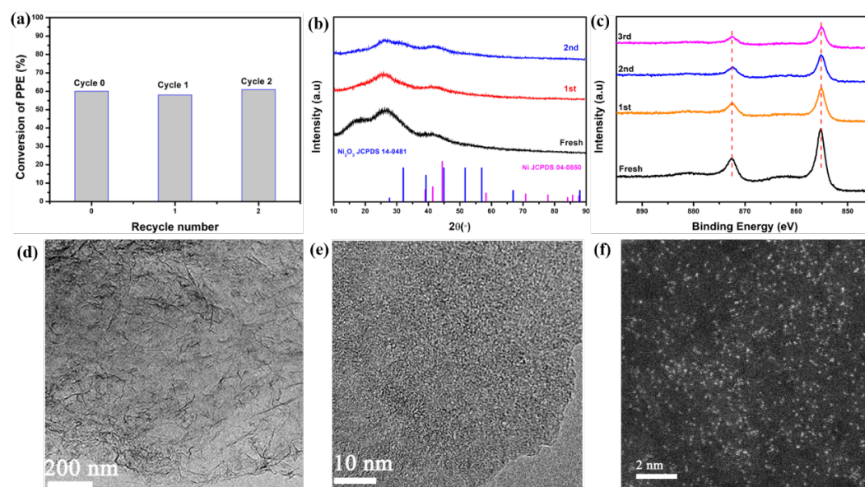


FIGURE 7 Recycling of Ni@N-C SAC in the catalytic hydrogenolysis of PPE and characterization of the used catalysts: (a) Recycling numbers (reaction conditions: 100 mg PPE, 20 mg catalyst, 20 ml isopropanol, stirring at 400 rpm, 200 °C, 5 h). (b) XRD pattern. (c) XPS Ni 2p. (d, e) TEM images. (f) Aberration-corrected HAADF-STEM image.

3.5 Catalytic Hydrogenolysis of Lignin

The high catalytic activity of Ni@N-C SAC toward the hydrogenolysis of lignin model compounds encouraged us to explore the application of Ni@N-C SAC in real lignin decomposition. In this work, birch organosolv lignin was employed as the substrate in the reaction. The yield of the aromatic monomers of Ni@N-C SAC is 31.2% with propylguaiacol and propysyringol as the main products (Table S4), which is about twice higher than those of Ni@NC (14.9%) and Raney nickel catalyst (12.3%), indicating Ni@N-C SAC is an efficient catalyst for lignin depolymerization. Figure 8 shows the 2D HSQC spectra of birch organosolv lignin and the corresponding oily products. The signals in the 2D HSQC spectra are labeled and summarized in Table S5. It is found that almost all the signals of A (β -O-4), B (β -5) and C (β - β) in lignin oil are disappeared after catalyzed reaction (Figure 8a vs Figure 8c) compared with that in lignin. In detail, the relative content of β -O-4 linkages in birch organosolv lignin was 42/100Ar, while the signals of A_α and A_β corresponding to benzylic alcohols and secondary alkyl protons of β -O-4 linkages almost completely disappeared, implying most β -O-4 linkages have been cleaved after reaction. Moreover, the signals of B (β -5) and C (β - β) in oily products are no longer observed, indicating that the stubborn C-C bonds are also cleaved after reaction. It is therefore interesting that Ni@N-C SAC shows high activity not only in cleaving C-O bonds, but also in cracking C-C bonds in lignin. It is also found that G and S units are observed with the amounts of 29% and 71% in fresh lignin. After reaction, the corresponding amounts were similarly 31% and 69%, respectively, suggesting that most of the aromatic units are not destroyed after reaction. As a comparison, Ni@NC exhibits lower depolymerization efficiency according to Figure 8b, and Figure 8e. Of which, the signals of A (β -O-4), B (β -5) and C (β - β) in lignin oil are still calculated 21%, 2% and 4%, respectively, and the corresponding amounts of the primary units (S and G) are also similarly to that in original lignin. The above results further confirm the higher catalytic activity of Ni@N-C SAC than Ni@NC in lignin depolymerization. GPC analysis gives another evidence of the excellent activity of Ni@N-C SAC. The GPC spectrum of birch organosolv lignin (Figure S10 and Table S6) shows a board molecular weight distribution with an average M_w of 4150 g/mol. After reaction, the average molecular weight of the two lignin oil samples catalyzed by

Ni@N-C SAC and Ni@NC are 590 g/mol and 1870 g/mol, respectively, which are much lower than that of birch organosolv lignin.

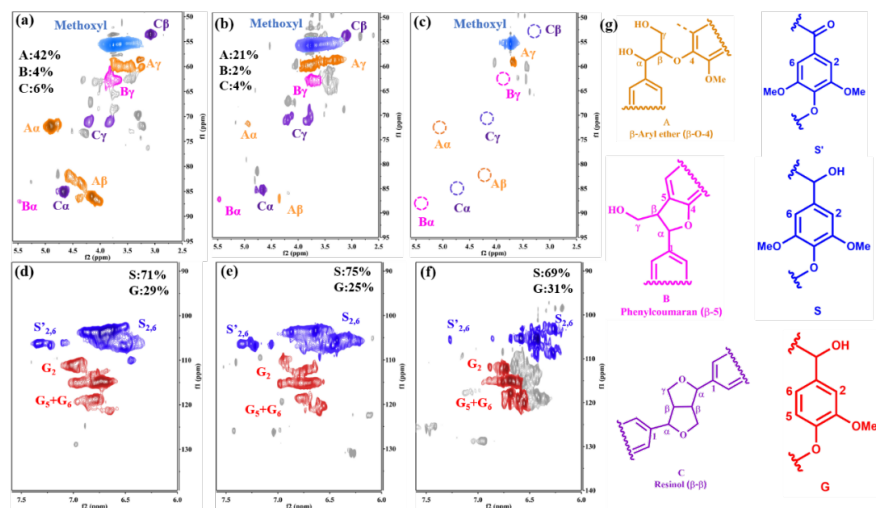


FIGURE 8 2D HSQC NMR spectra of birch organosolv lignin and the corresponding oily products: (a, d) birch organosolv lignin in DMSO-*d* 6 before reaction. (b, e) lignin oil after reaction with Ni@NC and (c, f) Ni@N-C SAC.

4 DISCUSSION

In this study, we demonstrate a chelation-anchored strategy for the synthesis of Ni@N-C SAC with a Ni loading up to 7.8 wt%. In the preparation of Ni@N-C SAC, Ni ions are first well dispersed by chelating with precursor containing OH or NH₂ groups, and then a two-step pyrolysis process not only restrains the growth of Ni particles but also introducing active N species into C carrier to form atomically dispersed Ni sites by providing N coordination site between the Ni and N species. The active site of Ni@N-C is a Ni-N₄ structure according to X-ray absorption fine structure analysis and computational modeling. Compared to Ni nano-cluster, the atomically dispersed Ni contributes to lower adsorption energies of Ni on the carrier, lower H₂ dissociation energy and energy barriers of the transition states in the hydrogenolysis process. Therefore, Ni@N-C SAC exhibits high catalytic activity in the hydrogenolysis of a lignin model compound and birch lignin. The 2D HSQC analysis of lignin and oily products reveals that Ni@N-C SAC shows high activity not only in cleaving C-O bonds, but also in cracking C-C bonds in lignin. This methodology opens up a facile strategy for the design of Ni@N-C SAC catalyst featuring high Ni loading and excellent catalytic activity in hydrogenolysis of both C-O and C-C bonds in lignin, highlighting the application potential not only in hydrocracking of large biomass molecules, but also in other catalytic reactions.

ACKNOWLEDGMENT

We thank financially supported by National Key Research and Development Plan of China (2019YFC1905301), the National Natural Science Foundation of China (No. 21776108, 22078115, 21690083).

AUTHOR CONTRIBUTIONS

The manuscript was written through contributions of all authors. All authors have given approval to the final version of the manuscript.

DATA AVAILABILITY STATEMENT

The data that support the findings of this study are available from the corresponding author upon reasonable request.

REFERENCES

1. Sun Z, Fridrich B, De Santi A, Elangovan S, Barta K. Bright Side of Lignin Depolymerization: Toward New Platform Chemicals. *Chem. Rev.* 2018;118(2):614-678.
2. Rafiee M, Alherech M, Karlen S. D, Stahl S. S. Electrochemical aminoxyl-mediated oxidation of primary alcohols in lignin to carboxylic acids: Polymer modification and depolymerization. *J. Am. Chem. Soc.* 2019;141(38):15266-15276.
3. Schutyser W, Renders A. T, Van den Bosch S, Koelewijn S. F, Beckham G. T, Sels B. F. Chemicals from lignin: an interplay of lignocellulose fractionation, depolymerisation, and upgrading. *Chem Soc Rev.* 2018;47(3):852-908.
4. Meng Q, Yan J, Wu R. et al. Sustainable production of benzene from lignin. *Nat Commun.* 2021;12(1):4534.
5. Wong S, Shu R, Zhang J, Liu H, Yan N. Downstream processing of lignin derived feedstock into end products. *Chem Soc Rev.* 2020;49(15):5510-5560.
6. Abu-Omar M. M, Barta K, Beckham G. T. et al. Guidelines for performing lignin-first biorefining. *Energy Environ Sci.* 2021;14(1):262-292.
7. Li C, Zhao X, Wang A, Huber G, Zhang T. Catalytic transformation of lignin for the production of chemicals and fuels. *Chem Rev.* 2015;115(21):11559-11624.
8. Wang S, Li W, Yang Y. et al. Unlocking Structure–Reactivity Relationships for Catalytic Hydrogenolysis of Lignin into Phenolic Monomers. *ChemSusChem.* 2020;13(17):4548-4556.
9. Peng C, Chen Q, Guo H. et al. Effects of extraction methods on structure and valorization of corn stover lignin by a Pd/C catalyst. *ChemCatChem.* 2017;9(6): 1135-1143.
10. Zhang B, Guo T, Liu Y. et al. Sustainable production of benzylamines from lignin. *Angew. Chem. Int.* 2021;60(38):20666-20671.
11. Arora S, Gupta N, Singh V. Improved Pd/Ru metal supported graphene oxide nano-catalysts for hydrodeoxygenation (HDO) of vanillyl alcohol, vanillin and lignin. *Green Chem.* 2020;22(6):2018-2027.
12. Yan J, Meng Q, Shen X. et al. Selective valorization of lignin to phenol by direct transformation of Csp²–Csp³ and C–O bonds. *Sci adv.* 2020;6(45):1951-1960.
13. Li L, Dong L, Liu X, Guo Y, Wang Y. Selective production of ethylbenzene from lignin oil over FeOx modified Ru/Nb₂O₅ catalyst. *Appl. Catal. B.* 2020;260:118143.
14. Gong J, Imbault A, Farnood R. The promoting role of bismuth for the enhanced photocatalytic oxidation of lignin on Pt-TiO₂ under solar light illumination. *Appl. Catal. B.* 2017;204:296-303.
15. Salakhum S, Yutthalekha T, Shetsiri S, Witoon T, Wattanakit C. Bifunctional and Bimetallic Pt–Ru/HZSM-5 Nanoparticles for the Mild Hydrodeoxygenation of Lignin-Derived 4-Propylphenol. *ACS Appl. Nano Mater.* 2019;2(2):1053-1062.
16. Guan W, Chen X, Zhang J, Hu H, Liang C. Catalytic transfer hydrogenolysis of lignin α -O-4 model compound 4-(benzyloxy) phenol and lignin over Pt/HNbWO₆/CNTs catalyst. *Renew Energy.* 2020;156(C):249-259.
17. Jiang L, Guo H, Li C, Zhou P, Zhang Z. Selective cleavage of lignin and lignin model compounds without external hydrogen, catalyzed by heterogeneous nickel catalysts. *Chem Sci.* 2019;10(16):4458-4468.
18. Song Q, Wang F, Cai J. et al. Lignin depolymerization (LDP) in alcohol over nickel-based catalysts via a fragmentation–hydrogenolysis process. *Energy Environ Sci.* 2013;6(3):994-1007.

19. Zhang B, Qi J, Li X. et al. Cleavage of lignin C–O bonds over a heterogeneous rhenium catalyst through hydrogen transfer reactions. *Green Chem.* 2019;21(20): 5556-5564.
20. Sirous-Rezaei P, Jae J, Cho K. et al. Insight into the effect of metal and support for mild hydrodeoxygenation of lignin-derived phenolics to BTX aromatics. *Chem Eng J* . 2019;**377** :120121.
21. Totong S, Laosiripojana W, Laosiripojana N, Daorattanachai P. Nickel and Rhenium Mixed Oxides-Doped Graphene Oxide (MOs/GO) Catalyst for the Oxidative Depolymerization of Fractionated Bagasse Lignin. *Ind. Eng. Chem. Res* . 2022;61(1):215-223.
22. Sergeev A. G, Hartwig, J. F. Selective, nickel-catalyzed hydrogenolysis of aryl ethers. *Science*. 2011;332(6028):439-443.
23. Wang M, Zhang X, Li H. et al. Carbon Modification of Nickel Catalyst for Depolymerization of Oxidized Lignin to Aromatics. *ACS Catal* . 2018;8(2):1614-1620.
24. Zhang J, Teo J, Chen X. et al. A Series of NiM (M=Ru, Rh, and Pd) Bimetallic Catalysts for Effective Lignin Hydrogenolysis in Water. *ACS Catal* . 2014;4(5):1574-1583.
25. Zhai Y, Li Z, Xu G. et al. Depolymerization of lignin via a non-precious Ni–Fe alloy catalyst supported on activated carbon. *Green Chem* . 2017;19(8):1895-1903.
26. Hannagan R. T, Giannakakis G, Flytzani-Stephanopoulos M, Sykes E. Single-atom alloy catalysis. *Chem Rev* . 2020;120(21):12044-12088.
27. Samantaray M. K, Pump E, Elia V. et al. The comparison between single atom catalysis and surface organometallic catalysis. *Chem Rev* . 2019;120(2):734-813.
28. Li Z, Ji S, Cao X. et al. Well-defined materials for heterogeneous catalysis: from nanoparticles to isolated single-atom sites. *Chem Rev* . 2019;120(2):623-682.
29. Mitchell S, Pérez-Ramírez J. Single atom catalysis: a decade of stunning progress and the promise for a bright future. *Nat Commun* . 2020;11(1):4312.
30. Liu W, Chen Y, Qi H. A Durable Nickel Single-Atom Catalyst for Hydrogenation Reactions and Cellulose Valorization under Harsh Conditions. *Angew. Chem.Int. Ed.* 2018;57(24):7071-7075.
31. Liu G, Robertson A. W, Meng-Jung Li M. MoS₂ monolayer catalyst doped with isolated Co atoms for the hydrodeoxygenation reaction. *Nat chem* . 2017;9:810-816.
32. Wang S, Zhang K, Li H, Xiao L, Song G. Selective hydrogenolysis of catechyl lignin into propenylcatechol over an atomically dispersed ruthenium catalyst. *Nat Commun* . 2021;12(1):416.
33. Shi J, Single-atom Co-doped MoS₂ monolayers for highly active biomass hydrodeoxygenation. *Chem* . 2017;2(4):468-469.
34. Mondelli C, Gozaydın G, Yan N, Pérez-Ramírez J. Biomass valorisation over metal-based solid catalysts from nanoparticles to single atoms. *Chem Soc Rev* . 2020;49: 3764-3782.
35. Tian S, Wang B, Gong W. et al. Dual-atom Pt heterogeneous catalyst with excellent catalytic performances for the selective hydrogenation and epoxidation. *Nat commun* . 2021;12:1-9.
36. Cao Y, Mao S, Li M, Chen Y, Wang Y. Metal/porous carbon composites for heterogeneous catalysis: old catalysts with improved performance promoted by N-doping. *ACS Catal* , 2017;7(12):8090-8112.
37. John P, Perdew K, Matthias E. Generalized Gradient Approximation Made Simple. *Phys Rev Lett*. 1996;77(18):3865-3868.
38. Kresse G, Joubert D. From ultrasoft pseudopotentials to the projector augmented-wave method. *Phys Rev B*. 1999;59(3):1758-1775.

39. Chadi D, Localized-orbital description of wave functions and energy bands in semiconductors. *Phys Rev B*. 1977;16:3572-3578.
40. Gong L, Zhang D, Lin C. et al. Catalytic Mechanisms and Design Principles for Single-Atom Catalysts in Highly Efficient CO₂ Conversion. *Adv. Energy Mater.* 2019; 9(44):1902625.
41. Wang J, Wei Z, Mao S, Li H, Wang Y. Highly uniform Ru nanoparticles over N-doped carbon: pH and temperature-universal hydrogen release from water reduction. *Energy Environ. Sci* . 2018;11:800-806.
42. Yuan S, Li T, Wang Y, et al. Double-adsorption functional carbon based solid acids derived from copolymerization of PVC and PE for cellulose hydrolysis. *Fuel*. 2019; 237: 895-902.
43. Fan L, Liu P, Yan X. et al. Atomically isolated nickel species anchored on graphitized carbon for efficient hydrogen evolution electrocatalysis. *Nat commun* . 2016;7 :1-7.
44. Zhao C, Dai X, Yao T. et al. Ionic exchange of metal-organic frameworks to access single nickel sites for efficient electroreduction of CO₂. *J.Am. Chem. Soc* . 2017;139(24):8078-8081.
45. Yang H, Huang S, Liu S. Atomically dispersed Ni(i) as the active site for electrochemical CO₂ reduction. *Nat. Energy*. 2018;3:140-147.
46. Zhao L, Zhang Y, Huang L. et al. Cascade anchoring strategy for general mass production of high-loading single-atomic metal-nitrogen catalysts. *Nat commun* . 2019;10:1278.
47. Fu F, Yang D, Zhang W, Wang H, Qiu X. Green self-assembly synthesis of porous lignin-derived carbon quasi-nanosheets for high-performance supercapacitors. *Chem Eng J* . 2020;392:123721.
48. Li S, Dong M, Yang J. et al. Selective hydrogenation of 5-(hydroxymethyl) furfural to 5-methylfurfural over single atomic metals anchored on Nb₂O₅. *Nat commun* . 2021;12:1-9.

SUPPORTING INFORMATION

The Supporting Information is available for this paper. Extraction of birch lignin, the results of catalytic tests, catalyst characterization and identification of aromatic monomers.

For Table of contents Use Only

